Korean J. Chem. Eng., 33(1), 305-311 (2016)
DOI: 10.1007/s11814-015-0141-8

pISSN: 0256-1115
eISSN: 1975-7220

A simple synthesis of $Ag_{2+x}Se$ nanoparticles and their thin films for electronic device applications

Duc Quy Vo*, Dang Duc Dung, Sunglae Cho**, and Sunwook Kim*,†**

*School of Chemical Engineering, University of Ulsan, Ulsan 680-749, Korea
**Department of Physics, University of Ulsan, Ulsan 680-749, Korea
(*Received 4 February 2015 • accepted 29 June 2015*)

Abstract−A simple method to synthesize silver selenide nanoparticles has been proposed. By changing the ratio of Se-oleylamine complex and silver acetate in the reacting mixture at different temperatures, both size and stoichiometry of the silver selenide particles could be successfully controlled. The size of the nanoparticles was adjusted by changing reaction temperatures. The synthesized silver selenide nanoparticles showed size changes from 3 to 10 nm when the corresponding reaction temperatures were 40-100 °C, respectively. In addition to the size change, the stoichiometry of the synthesized nanoparticles ($Ag_{2+x}Se$) could be adjusted by simply varying the ratio of Ag to Se precursors. Through XPS analyses the x value in $Ag_{2+x}Se$ was determined, and it changed between 0.54 and −0.03 by varying Ag/Se ratio from 2/0.75 to 2/4. The optical property of the nonstoichiometric $Ag_{2+x}Se$ nanoparticles was different from that of stoichiometric Ag_2Se nanoparticles, but showed the plasmon absorption of Ag-Ag network. The plasmon absorption was decreased with the increased concentration of the Se precursor. Finally, the $Ag_{2+x}Se$ thin film in this work showed large magnetoresistance and successfully applied to prepare high-performance Schottky diode. The $Ag_{2.06}Se$ film exhibited the magnetoresistance effect up to 0.9% at only 0.8 T at room temperature. The voltage drop and breakdown voltage of the Schottky diode were 0.5 V and 9.3 V, respectively.

Keywords: Silver Selenide, Optical Property, Magnetoresistance, Schottky Diode

INTRODUCTION

Silver selenide has been extensively investigated due to its many interesting and useful properties [1-17]. There are two stable solid phases for silver selenide: orthorhombic (β-Ag_2Se) and body-centered cubic (α-Ag_2Se). Moreover, this material shows a reversible first-order phase transition around 133 °C with a remarkable change in its electronic properties [1,2]. The low-temperature phase silver selenide (orthorhombic, <133 °C) is a narrow band-gap semiconductor with an energy gap of ~0.07 eV near 0 K [3], and it can be used as a basic material for various applications such as Schottky barriers, solar cells and electronic devices [5]. In addition to the above-mentioned applications, orthorhombic silver selenide (β-Ag_2Se) has been recognized as a promising candidate for the thermoelectric applications due to its large Seebeck coefficient (−150 mV K^{-1} at 300 K), high electrical conductivity (~2,000 S cm^{-1}), and low lattice thermal conductivity (~5 mW cm^{-1} K) [4]. The orthorhombic silver selenide also has been used as a themochromic material as well as a photosensitizer in photographic processing [5,7]. Contrary to the orthorhombic silver selenide, the high-temperature phase silver selenide (body-centered cubic, >133 °C) is a metallic compound with electrolyte characteristics [1,4] and may be useful as an additive in highly conductive glasses for manufacturing sensors, displays and batteries [3,13].

Various approaches have been utilized to prepare nanostructured Ag_2Se particles [1-4,7-13,18-22]. Ge and coworkers [1] used low-temperature positive microemulsion method to synthesize nearly uniform Ag_2Se nanoparticles. Ng et al. [4] prepared Ag_2Se nanocubes through the thermolysis of an organometallic precursor such as $[(PPh_3)_3Ag_2(SeC\{O\}Ph)_2]$. Ag_2Se nanofibers/nanowires have been synthesized using nanofiber/nanowire templates [8,9]. Su et al. [10] reported hydrothermal route to synthesize nanocrystalline Ag_2Se particles. And Jafari et al. [18] used sonochemical process for the synthesis of Ag_2Se nanoparticles by reacting two complexing agents in the presence of hydrazine as a reducing agent. However, previous methods to synthesize Ag_2Se nanoparticles possess a disadvantage, such as lack of controllability in terms of size and composition. Moreover, up to now, few procedures have been reported for the synthesis of Ag_2Se nanoparticles with size below 10 nm [1, 16,19-22] probably due to fast and strong reaction between Ag and Se precursors, even though the reaction was carried out in a short period of time at low temperature [1].

There have been numerous researches about extremely small particles, i.e., quantum dots (QDs), due to their great application potentials in the areas of photovoltaics, light emitting diodes, lasers, and biological imagings [21-30]. Recently, it has been reported that the ultra-small (sub-3 nm) Ag_2Se QDs possessed excellent near-infrared and photoluminescent characteristics for the utilization of bioimaging and biomedical areas [21,22]. Gu and coworkers [21] synthesized water-dispersible sub-3nm Ag_2Se QDs, and demonstrated that the near-infrared properties of Ag_2Se QDs could be used in bioimaging of living organism. And Dong et al. [22] uti-

†To whom correspondence should be addressed.
E-mail: swkim@ulsan.ac.kr

lized solvothermal method to synthesize highly photoluminescent Ag_2Se QDs, which showed colloidal stability, photostability and biocompatibility that those could be used in vivo deep imaging of organs and vascular structures. When the particle size decreases to the nanometer scale, quantization and surface effects become important to show drastic changes in physical and optical properties [24]. It has been reported that the photoluminescence (PL) emission and the UV-vis absorption peaks red-shifted with increasing particle size of nanoparticles [21]. Jasieniak et al. [25] investigated the size-dependent optical absorption coefficients of CdSe nanocrystals at the band-edge, and showed that the molar extinction coefficient at the band-edge increased with size. Quantum size effects in volume plasmon excitation of bismuth nanoparticles have been studied by Wang et al. [26], and they showed a blue shift in the plasmon peak position and an increase in peak width as decreasing particle diameters. Moreover, the melting point of a solid particle of 2-3 nm diameters is about a half of that for the solid with several-ten-nanometer size [31]. The low melting point of small sized nanoparticles is beneficial to fabricate corresponding thin films due to their low annealing temperatures [32]. In addition to the desirable property concerning particle size, the silver-rich silver selenide ($Ag_{2+x}Se$) nanoparticles are useful to prepare thin films with significant magnetoresistance characteristics which may be utilized for magnetoresistive sensors [33].

In this work, we report a simple method to synthesize silver-rich silver selenide nanoparticles with variable diameters ranging from 3 to 10 nm. The synthesis of the nanoparticles was controlled by slowing the reaction rate between Se and Ag precursors (Se-oleylamine complex and silver acetate). Furthermore, the stoichiometry of silver selenide nanoparticles could be controlled by simply varying the ratio of precursors (Ag/Se). The obtained products were used to fabricate $Ag_{2+x}Se$ thin film in order to measure magnetoresistance effect, and those were used to prepare high-performance Schottky diode.

EXPERIMENTAL

1. Chemicals

Oleylamine (70%), silver acetate (≥ 99%), selenium powder (Se, 99.5%) and hexane (≥99%) were obtained from Sigma-Aldrich Chemical Co. Acetone (Daejung Company, Korea, 99.5%) was used as an anti-solvent to recover nanoparticles from the reaction mixture. All the chemicals in the experiment were used as received without further purification.

2. Synthesis of $Ag_{2+x}Se$ Nanoparticles and Preparation of Thin Films

Se-oleylamine (Se-OLA) complex was used to react with silver acetate to synthesize silver selenide nanoparticles. The Se-OLA complex was prepared by reacting Se powder (1 g) with oleylamine (25 g) at 180 °C for 24 hrs. For a typical synthesis of $Ag_{2+x}Se$ (x= 0.23) nanoparticles with a diameter of ~5 nm, 0.4 g of silver acetate was first dissolved in 8.0 g of oleylamine (OLA), and then 2.42 g of the prepared Se-OLA complex solution was injected into the silver acetate/OLA solution. The reaction mixture was kept at 60 °C for 12 hrs. The size of the nanoparticles was adjusted by changing reaction temperature from 40 to 100 °C. To control the stoichiometry of Ag and Se in the produced nanoparticles, the concentration of silver acetate as well as that of Se-OLA complex was adjusted in the reaction mixture. After 12 hrs of reaction, 50 mL of acetone was added into a reacting solution to produce black solid particles [39] and those were redispersed in 40 mL of n-hexane.

To use as reference materials for the XPS analyses, OLA-coated Ag and Se particles were also prepared. OLA-coated Ag nanoparticles were synthesized using the procedure reported previously [34,35]. And OLA-coated Se particles were prepared by mixing Se powder (1 g) and oleylamine (25 g) at 180 °C for 24 hrs. After the solution was cooled to room temperature, the solid was collected using centrifuge and washed five times with acetone to remove free oleylamine. The film for the measurement of magnetoresistance and Hall resistance was prepared by spin-coating $Ag_{2.06}Se$ solution (7 wt% of $Ag_{2.06}Se$) onto intrinsic Si substrate at 2,000 rpm for 10 s and it was annealed at 250 °C for 0.5 hr. To fabricate Schottky diode, the n-Si(001) substrate was first cleaned with 10% HF solution to remove a SiO_2 layer on its surface [36]. Then, the substrate was partially covered with Scotch tape and was spin-coated with an $Ag_{2.06}Se$ solution (7 wt% of $Ag_{2.06}Se$) at 2,000 rpm for 10 s. After Scotch tape was removed, the spin-coated substrate was finally annealed at 250 °C for 0.5 hr. Two contacts were made by sputtering Au on $Ag_{2.06}Se$ and n-Si(001) surfaces.

3. Characterization

Transmission electron microscopy (TEM) and high resolution TEM (HRTEM) images were obtained by using a JEOL JEM-2100F operated at 200 kV. The X-ray diffraction (XRD) patterns were taken using a Rigaku D/Max 2500-V equipped with Cu Kα radiation (λ=1.5406 Å). Ultraviolet-visible (UV-vis) spectra were measured by Spectra Max Plus384 with a step of 5 nm. X-ray photoelectron spectroscope (XPS) data were taken using a Thermo Fisher Scientific K-alpha spectrometer. Fourier transform infrared (FT-IR) spectra were obtained by a Nicolet 380 spectrometer with a spectral resolution of 1 cm^{-1}. Using a physical property measurement system (PPMS), magnetoresistances and Hall resistances of the $Ag_{2.06}Se$ thin film coated on intrinsic-Si(001) were determined and the performance of a Schottky diode was characterized.

RESULTS AND DISCUSSION

1. Characteristics of Synthesized Silver Selenide Nanoparticles

Se powder was used here as a selenium source to synthesize silver selenide nanoparticles because it is cheaper and less toxic than the other sources such as H_2Se or $(CH_3)_2Se$. Figs. 1(a)-(d) are the TEM images of the silver selenide nanoparticles synthesized at different temperatures fixing the ratio of Ag/Se precursors with 2/1. It is clear that the size of the silver selenide nanoparticles could be controlled by changing reaction temperatures. The size of the synthesized nanoparticles changed from 3 to 5, 8 and 10 nm when corresponding reaction temperatures were 40, 60, 80, and 100 °C, respectively. HRTEM images in Figs. 1(e)-(f) clearly show the crystalline structure of the produced silver selenide nanoparticles. The increased particle size may be explained by the enhanced reaction rate between Ag and Se precursors and increased silver selenide concentration at high reaction temperature. The silver selenide nanoparticles synthesized at 40 and 60 °C were nearly uniform in particle size with-

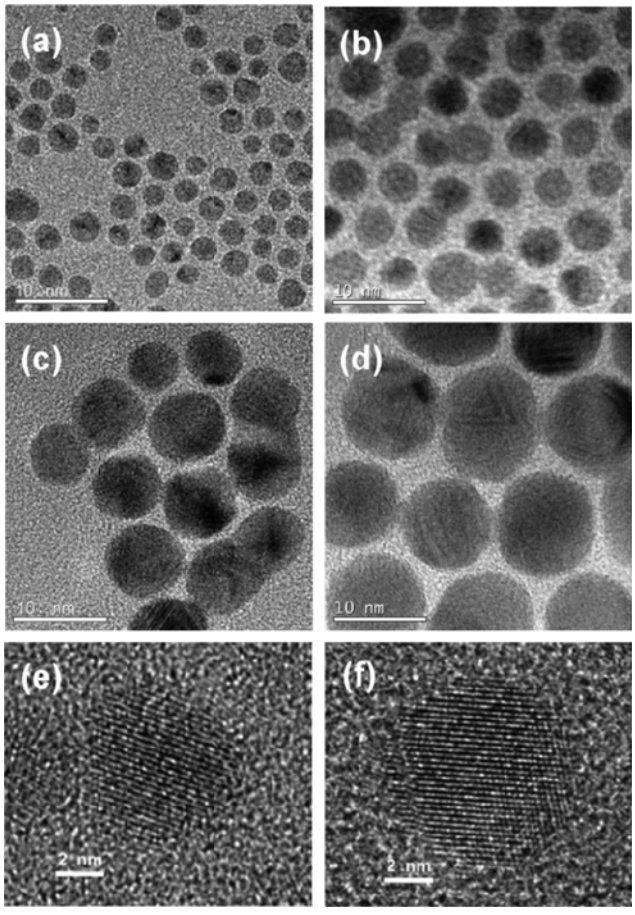

Fig. 1. TEM images of silver selenide nanoparticles synthesized at (a) 40, (b) 60, (c) 80, and (d) 100 °C for 12 hrs with the precursor ratio of Ag/Se=2/1. HRTEM images (e) and (f) are those of a single particle in (b) and (c), respectively.

out agglomeration. At higher reaction temperatures (80 and 100 °C), the nanoparticles tended to agglomerate because of a weak interaction between oleylamine and silver sites [34].

Figs. 2(a)-(d) show the XRD patterns of the silver selenide nanoparticles synthesized at different temperatures. The standard XRD pattern of the orthorhombic Ag_2Se (Fig. 2(e)) and those of Ag and Se powders (Figs. 2(f)-(g)) were also included for comparison. The position of all diffraction peaks of silver selenide in this work conforms to that of standard orthorhombic Ag_2Se peaks (β-Ag_2Se) [1]. Since the diffraction peaks of Ag and Se particles were not present in the XRD patterns (Figs. 2(a)-(d)), it could be concluded that the produced nanoparticles were only silver selenide without silver and selenium particles. By using the Scherrer equation [37], the average crystallite size was calculated as 3.5, 5.2, 8.2 and 10.4 nm when the silver selenide nanoparticles were synthesized at 40, 60, 80, and 100 °C, respectively. The average crystallite size was very close to the particle size determined from the TEM images. Even though the XRD patterns in this work are limited to those of the silver selenide nanoparticle synthesized by fixing the ratio of Ag/Se precursors with 2/1, the change of XRD patterns with varying stoichiometry of $Ag_{2+x}Se$ nanoparticles needs to be investigated further in the future communication.

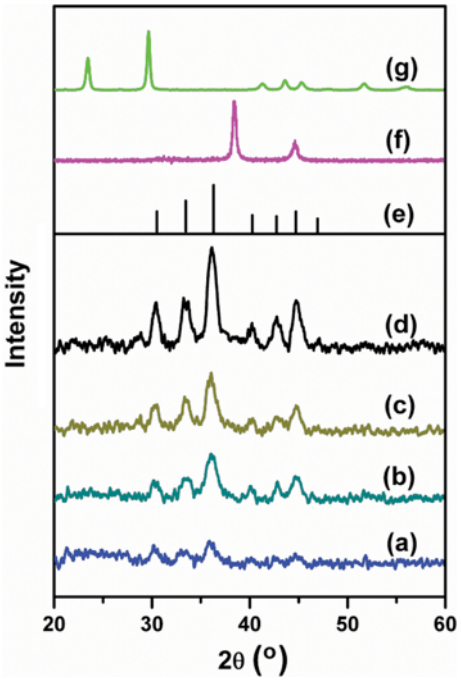

Fig. 2. XRD patterns of silver selenide nanoparticles synthesized at (a) 40, (b) 60, (c) 80, and (d) 100 °C for 12 hrs with the precursor ratio of Ag/Se=2/1. XRD pattern (e) is for the orthorhombic Ag_2Se standard (from JCPDS card, no. 241041), while (f) and (g) are those of Ag and Se powders.

FT-IR spectroscopy was used to characterize the surface chemistry of the silver selenide nanoparticles. As shown in Fig. 3, the FT-IR spectra of the silver selenide nanoparticles are almost similar to those of oleylamine. For instance, the silver selenide nanoparticles show the -NH_2 bending mode at 1,320-1,640 cm^{-1} and the CH_2 chain vibrations around 2,850-2,920 cm^{-1}, which are similar band positions of oleylamine [38,39]. The vibrations of Ag-Se bonds can be seen at a wavenumber below 800 cm^{-1} [1]. As a result, it can be concluded that oleylamine working as a stabilizer during the synthesis of the silver selenide nanoparticles covers the nanoparticle surfaces, which results in the interaction of nitrogen in oleylamine with surface atoms of Se and Ag.

2. Stoichiometry of Silver Selenide Nanoparticles

The stoichiometry of the silver-selenide nanoparticles was adjusted by simply varying the precursor ratio of Ag/Se in the reacting mixtures, and was determined through XPS analysis. The XPS technique is commonly used for the quantitative analysis of the material surfaces to the depth of 10 nm [42]. And it has been reported that the surface composition of semiconductor particles prepared by nonaqueous methods usually control1ed their stoichiometry [43,44]. Therefore, since the silver selenide nanoparticles synthesized in this work had diameters less than 10 nm, the stoichiometry of the synthesized silver selenide nanoparticles could be determined by the XPS analysis.

The N1s XPS spectra were used to determine the stoichiometry of synthesized nanoparticles. As mentioned previously in the FT-IR analysis (Fig. 3), oleylamine covered the silver selenide nanoparticles showing the interactions of nitrogen atoms with both Se and

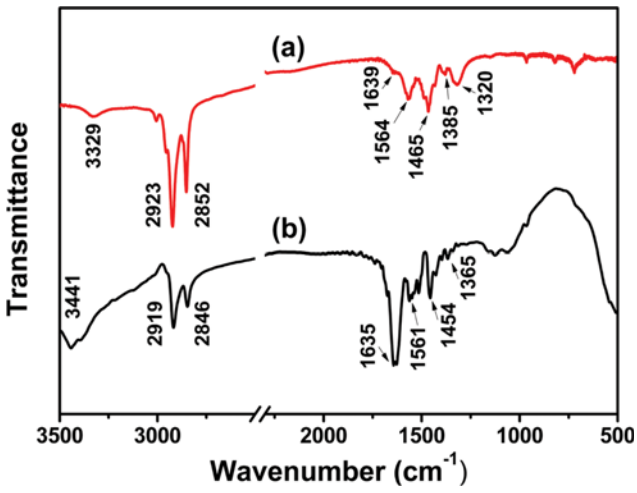

Fig. 3. FT-IR spectra of (a) oleylamine and (b) silver selenide nanoparticles synthesized at 60 °C for 12 hrs with the precursor ratio of Ag/Se=2/1.

Ag sites on the nanoparticle surface. Consequently, the N1s XPS spectra could be divided into two lines that were assigned to the binding energies of N coordinating with Ag (Ag-N-C) and Se (Se-N-C) peaked at 399.64 and 398.55 eV, respectively. As shown in Fig. 4, the number (peak area) of the Ag-N-C bonds decreased while that of the C-N-Se increased by changing Ag/Se ratios from 2/0.75 to 2/4 in the reaction mixture. For instance, when the precursor ratio (Ag/Se) was 2/0.75, the stoichiometry of the produced nanoparticles was determined to be $Ag_{2.54}Se$ (Fig. 4(a)) showing predominant number of Ag-N-C bonds on the surface. When the Ag/Se precursor ratio was 2/2, it led to the balance of Se-N-C and Ag-N-C bonds (Fig. 4(f)) and resulted in stoichiometric Ag_2Se nanoparticles. Increasing Ag/Se precursor ratio to 2/4, the number of Se-N-C bonds was larger than that of Ag-N-C (Fig. 4(g)) to produce $Ag_{1.97}Se$ nanoparticles. The XPS analyses showed that x value in $Ag_{2+x}Se$ changed as 0.54, 0.23, 0.12, 0.06, 0.02, 0 and −0.03 when the corresponding precursor ratio of Ag/Se was 2/0.75, 2/1.0, 2/1.25, 2/1.5, 2/1.75, 2/2 and 2/4, respectively. As a result, it can be said that the stoichiometry of the silver selenide nanoparticles may be controlled simply by adjusting Ag/Se precursor ratios.

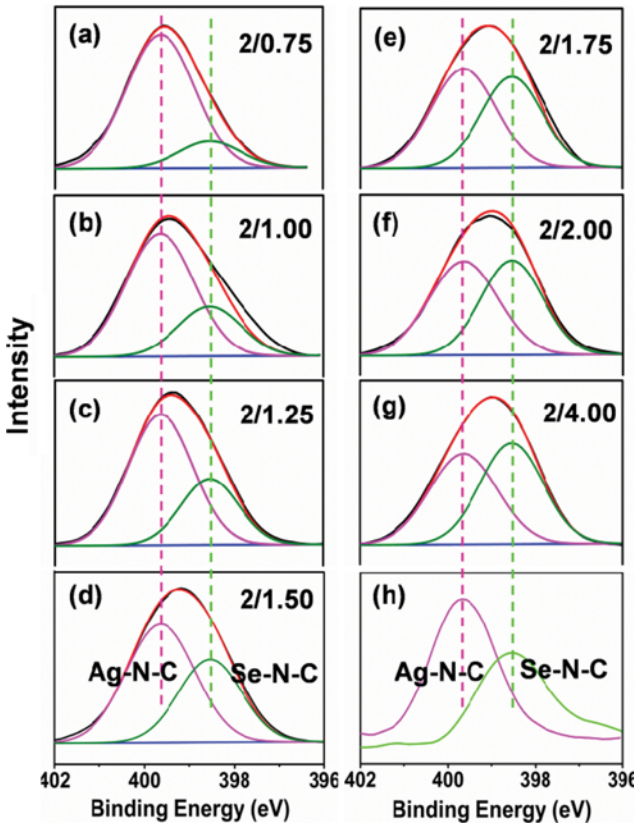

Fig. 4. (a)-(g) XPS N1s spectra of silver selenide nanoparticles synthesized from different ratios of Ag/Se precursors at 60 °C for 12 hrs. (h) XPS N1s spectra of oleylamine-coated Ag and oleylamine-coated Se particles (standard spectra of Ag-N-C and Se-N-C).

3. Optical Properties of Silver Selenide Nanoparticles

Fig. 5 shows the UV-vis spectra of the silver selenide nanoparticles synthesized at different temperatures using Ag/Se precursor ratio of 2/1. The silver selenides in Fig. 5 are $Ag_{2.23}Se$ nanoparticles with different size ranging from 3 to 10 nm. As can be expected, the spectra are different from that of stoichiometric Ag_2Se nanoparticles reported previously [20,40], but show the plasmon absorption of an Ag-Ag network [41]. Since free Ag nanoparticles did not form during the synthesis as confirmed by XRD analysis, it could be said that the plasmon absorptions in Fig. 5 were obtained solely from the silver selenide nanoparticles. It has been reported that the UV-vis and the plasmon peaks blue-shifted with decreasing the size of QDs [22,26,27]. However, in this work, the change of the plasmon absorption peaks for different sized silver selenide nanoparticles is insignificant, which requires further detailed investigation to elucidate the quantum size effect on the plasmon absorption of the silver selenide nanoparticles.

Fig. 6 shows the UV-vis absorption spectra of the $Ag_{2+x}Se$ nanoparticles with different stoichiometry obtained by varying Ag/Se precursor ratios. The plasmon absorption intensities decreased with increasing concentration of the Se precursor. For example, the plas-

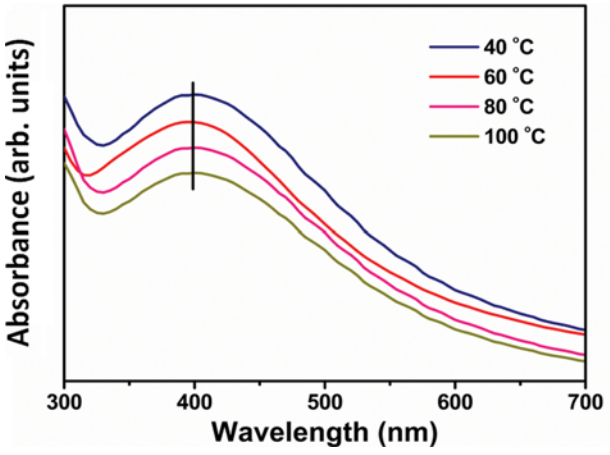

Fig. 5. UV-vis spectra of hexane-dispersed silver selenide nanoparticles synthesized at different temperatures for 12 hrs with the precursor ratio of Ag/Se=2/1.

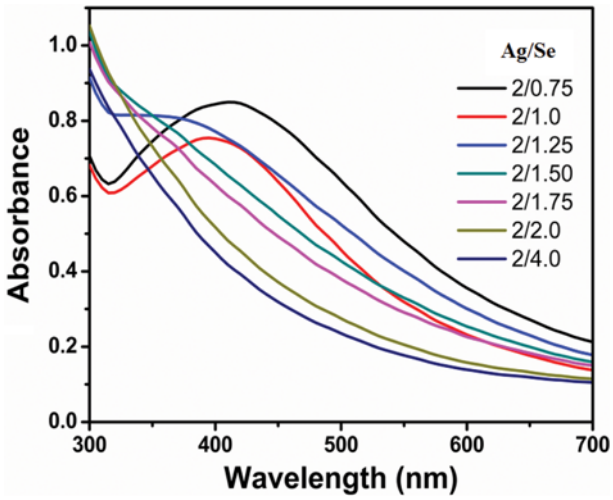

Fig. 6. UV-vis spectra of hexane-dispersed $Ag_{2+x}Se$ nanoparticles synthesized from different ratios of Ag/Se precursors at 60 °C for 12 hrs.

mon absorption intensities changed from 0.85 to 0.76 when the corresponding Ag/Se precursor ratios were 2/0.75 and 2/1.0, respectively. When the precursor ratio of Ag/Se was 2/0.75, the synthesized nanoparticles ($Ag_{2.54}Se$) showed clear characteristic plasmon absorption of silver. And the plasmon absorption was very low at the ratio of 2/1.5 ($Ag_{2.06}Se$) and disappeared completely at 2/2 (Ag_2Se). Since the XRD results showed that no free Ag nanoparticles were formed during the synthesis, the decrease in the plasmon absorption implied the diminution of the Ag-Ag network contained in the synthesized silver selenide nanoparticles [40].

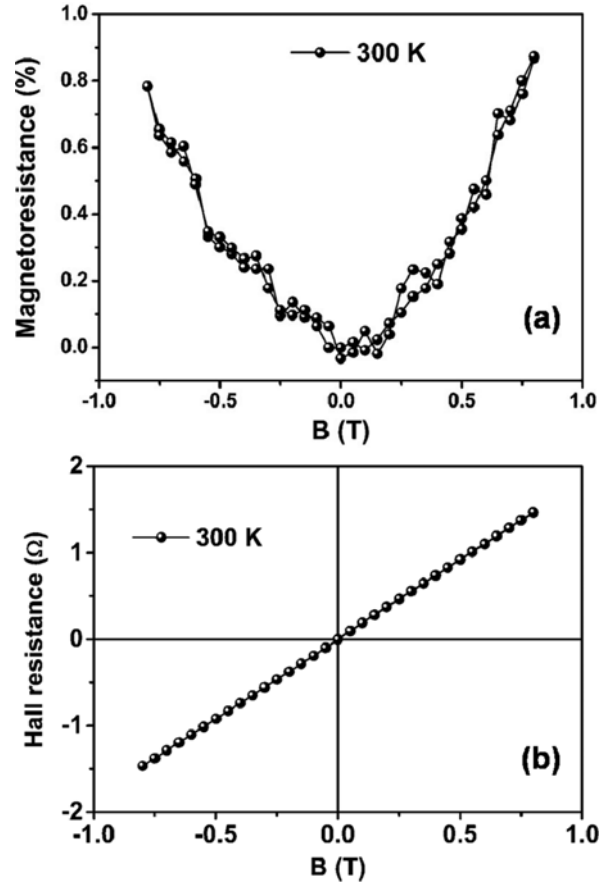

Fig. 7. (a) Magnetoresistance of the $Ag_{2.06}Se$ film as a function of applied magnetic field at room temperature. (b) Hall resistance of the $Ag_{2.06}Se$ film as a function of applied magnetic field at room temperature.

4. Physical Properties of a Thin Film Produced from $Ag_{2+x}Se$ Nanoparticles

Specific characteristics of $Ag_{2+x}Se$ particles are magnetoresistance and high carrier density properties [34,45-48], which may be useful in the application of a Schottky diode. Fig. 7(a) shows the magnetoresistance of an $Ag_{2.06}Se$ thin film versus applied magnetic field at room temperature. The positive magnetoresistance is caused by a Lorentz force that affects the carrier trajectories in conducting materials. The annealed film shows the magnetoresistance effect up to 0.8% at only 0.8 T at room temperature. The magnetoresistance effect in the present study can be competitive with those of $Ag_{2+x}Se$ films prepared by different methods reported previously [33,48,49].

Fig. 7(b) shows the Hall resistance as a function of applied magnetic field at room temperature. The positive slope indicated that the hole carrier was dominating in the β-$Ag_{2.06}Se$ film (p-type $Ag_{2.06}Se$) [50]. From the slope of Hall resistance versus applied magnetic field as well as the thickness of the β-$Ag_{2.06}Se$ film, the carrier density was estimated to be ~2.26×10^{19} cm^{-3} [50]. Simon et al. [51] obtained the n-type carrier of β-Ag_2Se at room temperature, but they could not find the p-type even at a temperature of 80 K. However, the Ag-rich silver selenide ($Ag_{2.06}Se$) could produce holes (p-type) due to diffusion of sliver atoms, which were substituted to selenium sites [52].

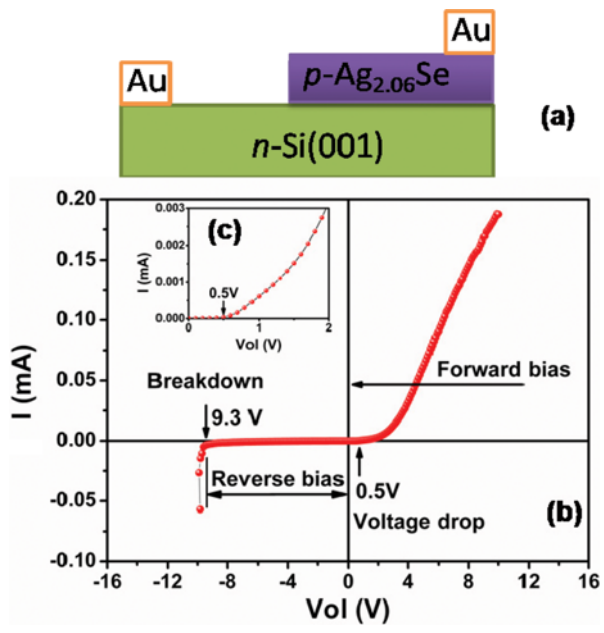

Fig. 8. (a) The schematic diagram of a Schottky diode with p-$Ag_{2.06}Se$/n-Si(001) contact. (b) Current in the diode as a function of the bias voltage at 300 K. (c) Forward I-V curve at low range of the bias voltage.

5. Performance of Schottky Diode Based on $Ag_{2+x}Se$ Nanoparticles

To utilize high carrier density properties of the $Ag_{2.06}Se$ thin film, we fabricated a Schottky diode [50,53,54]. The Schottky diode was prepared by the contact between the p-type $Ag_{2.06}Se$ and n-Si(001) as shown in Fig. 8(a). The I-V characteristics of the Schottky diode at 300 K are presented in Figs. 8(b)-(c). The I-V curve indicates the presence of a space charge region for the p-n contact of the device [50]. The appearance of the barrier potential in the junction between p-type $Ag_{2.06}Se$ and n-Si(001) was due to the difference of the potential of these two materials at the interface [50]. In the forward bias region, electrons were easily followed from n-type Si to p-type $Ag_{2.06}Se$ because the potential barrier decreased. The voltage drop was 0.5 V that could provide higher switching speed and better system efficiency [50]. In the revere bias, the reverse current was very small that p-$Ag_{2.06}Se$/n-Si(001) in this work satisfied one of the most important criteria of a Schottky diode [36,50]. When the applied reverse voltage continuously increased over the potential barrier, the breakdown of the current in the junction occurred. The breakdown voltage estimated to be about 9.3 V is the Zener diode voltage and this can be applied in several fields including voltage regulation [50].

CONCLUSIONS

Facile synthesis of silver selenide nanoparticles at low temperature has been performed through the reaction between Se-oleylamine complex and silver acetate. By changing reaction temperatures, the synthesized nanoparticles showed size changes such as 3, 5, 8, and 10 nm when the corresponding reaction temperatures were 40, 60, 80, and 100 °C, respectively. In addition to the adjustability of the particle size, the stoichiometry in the nanoparticles ($Ag_{2+x}Se$) could also be controlled by using different ratios of Ag/Se precursors. The x value in $Ag_{2+x}Se$ changed as 0.54, 0.23, 0.12, 0.06, 0.02, 0 and −0.03 when the corresponding precursor ratio of Ag/Se in the reaction was 2/0.75, 2/1.0, 2/1.25, 2/1.5, 2/1.75, 2/2 and 2/4, respectively. The optical property of the $Ag_{2+x}Se$ nanoparticles was different from that of stoichiometric Ag_2Se nanoparticles, but showed the plasmon absorption of Ag-Ag network. The plasmon absorption decreased with increasing concentration of the Se precursor.

The $Ag_{2+x}Se$ thin film in this work showed large magnetoresistance and was successfully applied to prepare high-performance Schottky diode. The annealed $Ag_{2.06}Se$ film exhibited the magnetoresistance effect up to 0.9% at only 0.8 T at room temperature. The voltage drop and breakdown voltage of the prepared Schottky diode were 0.5 V and 9.3 V, respectively. The reverse current was very small, such as 2 mA at the reverse voltage of 9.3 V.

ACKNOWLEDGEMENTS

This work was supported by the 2012 Research Fund of University of Ulsan.

REFERENCES

1. J.-P. Ge, S. Xu, L.-P. Liu and Y.-D. Li., *Chem. Eur. J.*, **12**, 3672 (2006).
2. C. H. B. Ng, H. Tan and W. Y. Fan, *Langmuir*, **22**, 9712 (2006).
3. S. K. Batabyal, C. Basu, A. R. Das and G. S. Sanyal, *Cryst. Growth Des.*, **4**, 509 (2004).
4. M. T. Ng, C. Boothroyd and J. J. Vittal, *Chem. Commun.*, **30**, 3820 (2005).
5. D. Li, Z. Zheng, Z. Shui, M. Long, J. Yu, K. W. Wong, L. Yang, L. Zhang and W. M. Lau, *J. Phys. Chem. C*, **112**, 2845 (2008).
6. S. P. Anthony, *Mater. Lett.*, **63**, 773 (2009).
7. S.-Y. Zhang, C.-X. Fang, W. Wei, B.-K. Jin, Y.-P. Tian, Y.-H. Shen, J.-X. Yang and H.-W. Gao, *J. Phys. Chem. C*, **111**, 4168 (2007).
8. B. Gates, B. Mayers, Y. Wu, Y. Sun, B. Cattle, P. Yang and Y. Xia, *Adv. Funct. Mater.*, **12**, 679 (2002).
9. H. Wang and L. Qi, *Adv. Funct. Mater.*, **18**, 1249 (2008).
10. H. Su, Y. Xie, B. Li and Y. Qian, *Mater. Res. Bull.*, **35**, 465 (2000).
11. Y. J. Glanville, D. G. Narehood, P. E. Sokol, A. Amma and T. Mallouk, *J. Mater. Chem.*, **12**, 2433 (2002).
12. Y.-I. Yan, X.-F. Qian, H.-J. Xu, J.Yin and Z.-K. Zhu, *Inorg. Chem. Commun.*, **6**, 34 (2003).
13. W. Wang, Y. Geng, Y. Qian, M. Ji and Y. Xie, *Mater. Res. Bull.*, **34**, 877 (1999).
14. D. T. Schoen, C. Xie and Y. Cui, *J. Am. Chem. Soc.*, **129**, 4116 (2007).
15. V. Buschmann, G. Van Tendeloo, Ph. Monnoyer and J. B. Nagy, *Langmuir*, **14**, 1528 (1998).
16. A. Sahu, A. Khare, D. D. Deng and D. J. Norris, *Chem. Commun.*, **48**, 5458 (2012).
17. A. Panneerselvam, C. Q. Nguyen, M. A. Malik, P. O'Brien and J. Raftery, *J. Mater. Chem.*, **19**, 419 (2009).
18. M. Jafari, M. Salavati-Niasari and A. Sobhani, *Micro & Nano Lett.*, **8**, 508 (2013).
19. D. Wang, T. Xie, Q. Peng and Y. Li, *J. Am. Chem. Soc.*, **130**, 4016 (2008).
20. D. H. Son, S. M. Hughes, Y. Yin and A. P. Alivisatos, *Science*, **306**, 1009 (2004).
21. Y.-P. Gu, R. Cui, Z.-L. Zhang, Z.-X. Xie and D.-W. Pang, *J. Am. Chem. Soc.*, **134**, 79 (2012).
22. B. Dong, C. Li, G. Chen, Y. Zhang, Y. Zhang, M. Deng and Q. Wang, *Chem. Mater.*, **25**, 503 (2013).
23. M. A. El-Sayed, *Acc. Chem. Res.*, **37**, 326 (2004).
24. S. Neeleshwar, C. L. Chen, C. B. Tsai, Y. Y. Chen, C. C. Chen, S. G. Shyu and M. S. Seehra, *Phys. Rev. B*, **71**, 201307 (2005).
25. J. Jasieniak, L. Smith, J. van Embden, P. Mulvaney and M. Califano, *J. Phys. Chem.*, **113**, 19468 (2009).
26. Y. W. Wang, J. S. Kim, G. H. Kim and K. S. Kim, *Appl. Phys. Lett.*, **88**, 143106 (2006).
27. J. M. Luther, P. K. Jain, T. Ewers and A. P. Alivisatos, *Nat. Mater.*, **10**, 361 (2011).
28. M. M. Alvarez, J. T. Khoury, T. G. Schaaff, M. N. Shafigullin, I. Vezmar and R. L. Whetten, *J. Phys. Chem.*, **101**, 3706 (1997).
29. S. Park, M.-K. Son, S.-K. Kim, M.-S. Jeong, K. Prabakar and H.-J. Kim, *Korean J. Chem. Eng.*, **30**, 2088 (2013).
30. H. C. Kim, C. Yoon, Y.-G. Song, Y.-J. Kim and K. Lee, *Korean J. Chem. Eng.*, **32**, 563 (2015).
31. P. Buffat and J. P. Borel, *Phys. Rev. A*, **13**, 2287 (1976).
32. Y. Li, Y. Wu and B. S. Ong, *J. Am. Chem. Soc.*, **127**, 3266 (2005).
33. J. Janek, B. Mogwitz, G. Beck, M. Kreutzbruck, L. Kienle and C. Korte, *Prog. Solid State Chem.*, **32**, 179 (2004).

34. H. Hiramatsu and F. E. Osterloh, *Chem. Mater.*, **16**, 2509 (2004).
35. S. Sun and H. Zeng, *J. Am. Chem. Soc.*, **124**, 8204 (2002).
36. S. Kumar and D. Kanjilal, *Nucl. Instr. Meth. Phys. Res. B*, **248**, 109 (2006).
37. X. Chen and S. S. Mao, *Chem. Rev.*, **107**, 2891 (2007).
38. H. G. Bagaria, E. T. Ada, M. Shamsuzzoha, D. E. Nikeles and D. T. Johnson, *Langmuir*, **22**, 7732 (2006).
39. D. Q. Vo, E.-J. Kim and S. Kim, *J. Colloid Interface Sci.*, **337**, 75 (2009).
40. J. Zhang, Y. Tang, L. Weng and M. Ouyang, *Nano Lett.*, **9**, 4061 (2009).
41. M. Chen, Y.-G. Feng, X. Wang, T.-C. Li, J.-Y. Zhang and D.-J. Qian, *Langmuir*, **23**, 5296 (2007).
42. E. N. Kaufmann, *Common concepts in materials characterization*, Wiley, New York (2002).
43. A. J. Morris-Cohen, M. T. Frederick, G. D. Lilly, E. A. McArthur and E. A. Weiss, *J. Phys Chem. Lett.*, **1**, 1078 (2010).
44. A. A. Guzelian, J. E. B. Katari, A. V. Kadavanich, U. Banin, K. Humad, E. Juban, A. P. Alivisatos, R. H. Wolters, C. C. Arnold and J. R. Heath, *J. Phys. Chem.*, **100**, 7212 (1996).
45. F. Yang, S. Xiong, Z. Xia, F. Liu, C. Han and D. Zhang, *Semicond. Sci. Technol.*, **27**, 125017 (2012).
46. J. Jasieniak and P. Mulvaney, *J. Am. Chem. Soc.*, **129**, 2841 (2007).
47. B. Mogwitz, C. Korte, J. Janek, M. V. Kreutzbruck and L. Kienle, *J. Appl. Phys.*, **101**, 043510 (2007).
48. M. V. Kreutzbruck, G. Lembke, B. Mogwitz, C. Korte and J. Janek, *J. Phys. Rev. B*, **79**, 035204 (2009).
49. S. S. Monoharan, S. J. Prasanna, D. E. Kiwitz and C. M. Schneider, *Phys. Rev. B*, **63**, 212405 (2001).
50. L. J. Brillson, *Contacts to semiconductors: fundamentals and technology*, William Andrew Publishing, New York (1993).
51. R. Simon, R. C. Bourke and E. H. Lougher, *Adv. Energy Convers.*, **3**, 481 (2001).
52. Y. Tang and M. Ouyang, *Nat. Mater.*, **6**, 754 (2007).
53. T.-H. Gil, H.-S. Kim, J.-W. Lee and Y.-S. Kim, *Solid-State Electron.*, **50**, 1510 (2001).
54. M. B. Reddy, A. A. Kumar, V. Janardhanam, V. R. Reddy and P. N. Reddy, *Curr. Appl. Phys.*, **9**, 972 (2009).